ChemComm

ROYAL SOCIETY OF CHEMISTRY

COMMUNICATION

View Article Online
View Journal | View Issue

Cite this: *Chem. Commun.*, 2020, **56**, 8758

Received 30th April 2020,
Accepted 15th June 2020

DOI: 10.1039/d0cc03111a

rsc.li/chemcomm

Highly stable 3D porous HMOF with enhanced catalysis and fine color regulation by the combination of d- and p-ions when compared with those of its monometallic MOFs†

Jiao Liu,[a] Ying Zhao,[b] Li-Long Dang,[b] Guoping Yang, *[a] Lu-Fang Ma, *[ab] Dong-Sheng Li [c] and Yaoyu Wang [a]

In this study, two new monometallic organic frameworks (MOFs), namely $\{[Zn_{1.5}L(NMP)(H_2O)]\cdot H_2O\}_n$ (1) and $\{[Pb_2L_2(H_2O)_2]\cdot H_2O\}_n$ (2), were synthesized for the first time by a new bifunctional N,O-containing 2-(1*H*-tetrazol-5-yl)terephthalic acid (H_2L) ligand. Then, based on the HSAB principle, another porous Pb–Zn heterometallic organic framework (HMOF), namely $\{[PbZn_{0.5}L(H_2O)]\cdot 0.5NMP\cdot H_2O\}_n$ (3), was successfully obtained for the first time by combining Pb(II) and Zn(II) ions with H_2L. The MOFs 1 and 2 are 3D densely packed frameworks, whereas the HMOF 3 is a porous 3D framework (28.9% porosity) with 1D open channels modified by Lewis basic sites (exposed N atoms) and Lewis acidic sites (unsaturated bimetallic sites). The HMOF 3 has a strong boiling water/acid–base resistance (pH = 2–12) and shows an enhanced high-efficiency catalytic effect for CO_2 conversion (98%) under ambient temperature and pressure conditions. In addition, fine color regulations of the MOFs were successfully realized by doping different kinds of metal ions into them. This study aims to provide a new way and field of vision for the construction of HMOFs and their multi-functional materials.

Heterometallic–organic frameworks (HMOFs) formed by the assembly of two or more kinds of metal ions with organic ligands have attracted significant attention owing to their structural and functional advantages.[1–3] Especially, the introduction of second metal ions into the framework as additional unsaturated sites can directly and effectively enhance the affinity of reactants to the host frameworks, such as CPM-200s, of HMOFs.[4] However, in recent years, only few HMOFs with great catalytic properties have been reported, for instance, $[Th_{48}Ni_6]$ nanocages,[5] Ni–Co-MOF,[6] and $Zn_4Ln_3L_4$[7] have presented relatively high catalytic efficiency under mild conditions. Compared with the case of MOFs, very few studies have been reported on HMOFs. The key problem is when two kinds of metal ions react with the same ligand, the formation of monometallic MOFs is more likely than that of HMOFs. According to the hard–soft acid–base (HSAB) principle, the Pb(II) and Zn(II) ions have different coordination abilities to the electron-donating O and N atoms; this provides possibilities of competition between different metal ions and atoms possessing a lone pair of electrons in ligands. That is, the Pb(II) ions are more easily coordinated with oxygen atoms to form rod-like metal chains or clusters, leading to non-porous MOFs with densely packed structures;[8,9] however, the Zn(II) ions are more prone to coordinate with N atoms and yield porous MOFs when compared with the case of the Pb(II) ions. Therefore, there is an assumption that the Zn(II) and Pb(II) ions can combine together to prepare highly stable porous HMOFs with improved performances when compared with those of their monometallic MOFs.

In addition, the selection of ligands is of great importance for the construction of HMOFs. To date, only few smaller types of ligands, such as carbonyl, CN^-, and $N(CN)^{2-}$,[1,10] have been used to build functional HMOFs. Based on the these discussions, a new bifunctional N,O-containing 2-(1*H*-tetrazol-5-yl)terephthalic acid (H_2L) ligand was designed to produce new HMOFs with high porosity. Herein, two new monometallic MOFs, namely $\{[Zn_{1.5}L(NMP)(H_2O)]\cdot H_2O\}_n$ (**1**) and $\{[Pb_2L_2(H_2O)_2]\cdot H_2O\}_n$ (**2**), were synthesized for the first time and showed 3D densely packed frameworks. Then, a new porous Pb–Zn HMOF, namely

[a] *Key Laboratory of Synthetic and Natural Functional Molecule of the Ministry of Education, Shaanxi Key Laboratory of Physico-Inorganic Chemistry, College of Chemistry & Materials Science, Northwest University, Xi'an 710127, P. R. China. E-mail: ygp@nwu.edu.cn*

[b] *College of Chemistry and Chemical Engineering, Henan Key Laboratory of Function-Oriented Porous Materials, Luoyang Normal University, Luoyang 471934, P. R. China. E-mail: mazhuxp@126.com*

[c] *College of Materials and Chemical Engineering, Hubei Provincial Collaborative Innovation Center for New Energy Microgrid, Key Laboratory of Inorganic Nonmetallic Crystalline and Energy Conversion Materials, China Three Gorges University, Yichang 443002, P. R. China*

† Electronic supplementary information (ESI) available: The syntheses of crystals, X-ray crystallographic data in CIF format, additional structural figures, the ^{1}H NMR spectra, and bond length/angle tables. CCDC 1998756–1998758. For ESI and crystallographic data in CIF or other electronic format see DOI: 10.1039/d0cc03111a

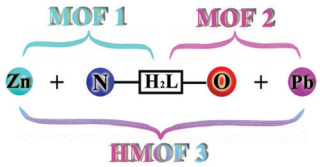

Scheme 1 The synthetic route of the MOFs **1–2** and HMOF **3**.

$\{[PbZn_{0.5}L(H_2O)]\cdot 0.5NMP\cdot H_2O\}_n$ (**3**), was produced by combining Pb(II) and Zn(II) ions with H_2L *via* a reaction. Compared with the MOFs **1** and **2**, the HMOF **3** is a 3D porous framework with 1D open channels modified by Lewis basic sites (LBSs, exposed N atoms) and Lewis acidic sites (LASs, unsaturated bimetallic sites) and has high stability in a boiling water and acid/base environment. As a result, the HMOF **3** can be explored as an extraordinary catalyst for CO_2 fixation under ambient temperature and pressure conditions. Furthermore, fine color regulations were realized by doping different metal ions into these MOFs; that is, the MOFs **1** and **2** showed a relatively strong single blue and weak yellow emission, respectively, whereas the HMOF **3** exhibited a near white emission when applied in photoemitters.

The solvothermal reactions of Zn(II)/Pb(II) ions with the H_2L ligand afforded the monometallic MOFs **1** and **2**, whereas the HMOF **3** was directly obtained by a one-pot reaction of Pb(II) and Zn(II) ions at an equal molar ratio with H_2L (Scheme 1). Note that the HMOF **3** cannot be synthesized by a stepwise construction strategy; this may be due to the existence of strong coordination bonds in the MOFs **1** and **2**, and it is thus difficult to break the original bonds and form new bonds during the reaction. The MOF **1** crystallizes in a monoclinic crystal system with the $P2(1)/n$ space group. X-ray single-crystal structure determination revealed that the basic unit of the MOF **1** comprises one Zn1(II) and half Zn2(II) ions (100 and 50% site occupancies, respectively), one L^{2-}, one coordinated NMP molecule, one H_2O molecule, and one guest H_2O molecule (Fig. 1a). Zn1(II) is four-coordinated by three O atoms and one N atom in a distorted tetrahedral fashion, and the six-coordinated Zn2(II) ion adopts distorted octahedral coordination geometries. The carboxylates of L^{2-} are coordinated with the Zn(II) ions in $\eta^1{:}\eta^0$, $\eta^1{:}\eta^1{:}\mu_2$ coordination fashions (Fig. S1a, ESI†). Moreover, 1D pores formed by $[Zn_6(L)_6(NMP)_2]$ exist in **1** (Fig. S1b, ESI†). The coordinated NMP molecules remain in the middle of the pores. Along the *a*-axis, these 1D pores are extended by L^{2-} into a 3D framework loaded with H_2O molecules (Fig. S1c, ESI†). In addition, this 3D framework can form a rare tri-nodal (2,3,4)-connected ***ins*** topological net with the symbol $(6^3)(6^5{\cdot}8)$ (Fig. S1d, ESI†).[11]

The MOF **2** belongs to the triclinic $P\bar{1}$ space group. The asymmetric unit of **2** consists of two Pb(II) ions, two L^{2-}, two coordinated H_2O molecules, and one guest H_2O molecule (Fig. 1b). Considering the primary Pb–O bonds of up to 2.7 Å, Pb1 and Pb2 can be described as four- and five-coordinated modes, respectively. All the Pb(II) ions in **2** are in hemidirected geometries, indicating the existence of stereochemically active 6s lone pair electrons. In the void direction of the Pb coordination geometry, Pb1(II) is weakly coordinated to O1, O4, O9, and O10 with $\eta^2{:}\eta^1{:}\mu_2$ modes to link the Pb(II) ions to form a 1D infinite chain motif (Fig. S2a, ESI†), and these 1D chains are further extended by L^{2-} to afford a 3D densely packed framework (Fig. S2b and c, ESI†). Topologically, L^{2-} can be considered as a 5-connected node (Fig. 3a), and the two kinds of Pb(II) ions are regarded as 4 and 6-connected node; thus, the 3D framework forms a new tetra-nodal (4,5,5,6)-connected topology with the symbol $(4^{11}{\cdot}6^4)(4^6{\cdot}6^4)(4^7{\cdot}6^3)(4^9{\cdot}6^6)$ (Fig. S2d, ESI†).

The HMOF **3** crystallizes in the monoclinic $C2/c$ space group and exhibits a porous 3D framework with double LBSs and LASs. The asymmetric unit contains one Pb(II) and half Zn(II) ions (100 and 50% site occupancies, respectively), one L^{2-} ligand, one coordination H_2O molecule, one guest H_2O molecule, and half NMP molecule (Fig. 2a). Regardless of the weak coordination of the Pb–O bond (2.847 Å), the six-coordinated Pb(II) ion is bridged by one tetrazolate N atom and five O atoms to form a distorted octahedral coordination geometry, whereas the Zn(II) ion is unsaturated four-coordinated with two tetrazolate N atoms and two bridged carboxylate O atoms, displaying a tetrahedral configuration. Furthermore, one L^{2-} links four Pb(II) and two Zn(II) ions by the tetrazolate group and two carboxylates with the $\eta^1{:}\eta^1{:}\mu_2$ and $\eta^2{:}\eta^2{:}\mu_3$, modes (Fig. S3a, ESI†); this forms planar bimetallic chains as secondary building units (SBUs) (Fig. S3b, ESI†). Along the *c*-axis, these SBUs are further linked by L^{2-} to produce a 3D framework including a 1D open channel with the window sizes of *ca.* 8.6 × 11.6 $Å^2$, where the LBS and LAS are decorated on the porous surface (Fig. 2b). The

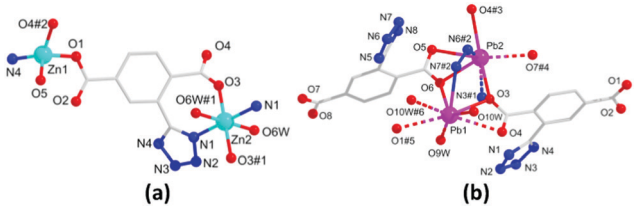

Fig. 1 Coordination environments of the Zn(II) ions and Pb(II) ions in **1** (a) and **2** (b); symmetry codes for **1**: #1: 2 − *x*, 1 − *y*, 1 − *z* and #2: 1.5 − *x*, 0.5 + *y*, 0.5 − *z*; for **2**: #1: 1 − *x*, 1 − *y*, 1 − *z*; #2: −*x*, −*y*, 2 − *z*; #3: *x* − 1, *y*, *z*; #4: *x*, 1 + *y*, *z*; #5: *x*, *y* − 1; *z*; and #6: 1 − *x*, −*y*, 2 − *z*.

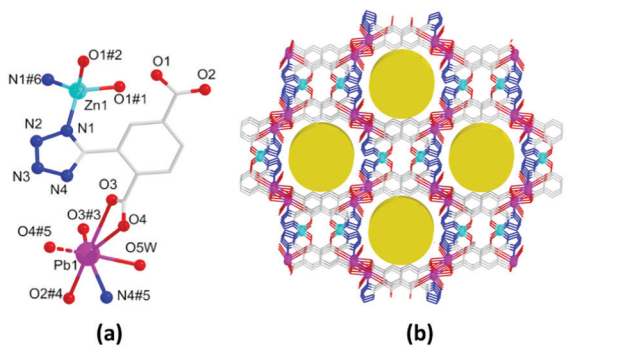

Fig. 2 (a) Coordination environment of the Pb(II) and Zn(II) ions in **3**; symmetry codes: #1: *x*, 1 − *y*, −0.5 + *z*; #2: 1 − *x*, 1 − *y*, 1 − *z*; #3: 0.5 − *x*, 1.5 − *y*, −*z*; #4: 0.5 − *x*, 0.5 + *y*, 0.5 − *z*; #5: 0.5 − *x*, 1.5 − *y*; 1 − *z*; and #6: 1 − *x*, *y*, 0.5 − *z*. (b) The 3D porous framework of **3**.

effective porosity of **3** is 28.9% regardless of the free solvent molecules. Topologically, the Pb(II) and two Zn(II) ions can be simplified as a 4-connected node to be further linked by hexadentate L^{2-} ligands into a new trinodal (4,4,6)-connected topology with the point symbol $(4^4{\cdot}6^2)_3(4^9{\cdot}6^6)_2$ (Fig. S3d, ESI†).

The thermogravimetric analysis curve of **3** shows that there is an 8.8% weight loss at ~32–132 °C, which corresponds to the escape of dissociative solvent molecules (calcd 8.0%) (Fig. S4, ESI†). The main skeleton of the structure remains stable in the temperature range of ~132–303 °C and then quickly collapses. Powder X-ray diffraction (PXRD) indicated that the synthesized solid samples **1–3** have high purity (Fig. S5, ESI†). The stability of the host framework is of great importance for the application of a MOF as catalyst thus, the chemical and thermal stabilities of the HMOF **3** were carefully tested for further studying the properties of the HMOF (Fig. 3). The PXRD analyses showed that the HMOF not only is very stable in boiling water, but also has a strong acid–base resistance, which may avoid the potential Pb(II) contamination of the environment during the application process. The unusual chemical and thermal stabilities of the HMOF **3** should be ascribed to its unique structure because the bimetallic chains acting as the SBUs may be more stable, and more importantly, the several free basic N atoms present in its structure prevent the collapse of the HMOF **3** under strong acidic conditions.[3]

In order to more directly and effectively reduce CO_2 in the atmosphere, the conversion of CO_2 into more valuable chemicals, such as formic acid, dimethyl carbonate, and carbonates, is often considered.[12–14] The carbonate formed by the cycloaddition of CO_2 to epoxides has been widely used in the pharmacy and chemical industry and has attracted widespread attention in recent years. To date, only few studies have been reported on the synthesis of HMOFs with bimetallic nodes as Lewis acids.[15,16] High-density LBSs and LASs are modified on the pore surface of **3**, which is then effectively applied for the capture of CO_2 to obtain more valuable products. Herein, due to the existence of guest molecules in the channels of **3**, the removal of free molecules was excluded to release the active sites before the catalytic reaction. The synthesized **3** was first soaked in CH_2Cl_2 and then heated to 100 °C for 4 h under high vacuum to obtain desolvated **3a**, and the infrared spectra demonstrated that there is no C═O vibration of the NMP molecules in **3** (Fig. S6, ESI†).

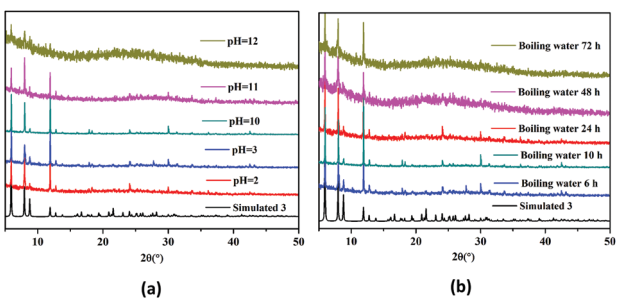

Fig. 3 The stability of **3**. (a) PXRD patterns obtained in an acid/base solution with pH = 2–12. (b) The PXRD patterns of boiling water *vs.* time.

Table 1 Various carbonates obtained from the catalysis of epoxides by **3a** for 12 h

Entry	Epoxide	Product	Catalyst	Yield (%)
1			TBAB	5.4
2			**3a**	9.9
3			**3a**/TBAB	98
4			**3a**/TBAB	98
5	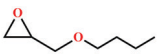	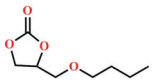	**3a**/TBAB	56
6			**3a**/TBAB	26

Condition: epoxides (20 mmol), **3a** (0.2 mmol), TBAB (2 mmol), and ambient temperature and pressure.

Based on the abovementioned discussion, the catalytic performance of **3a** was investigated in the coupling reaction of CO_2 with various epoxides at ambient temperature (Scheme S1, ESI†). After a 12 h reaction in the presence of tetra-*n*-butyl ammonium bromide (TBAB) or **3a** as a catalyst, the yield of the product was low (Table 1). Moreover, when **3a** was used as a catalyst and TBAB was used as a co-catalyst, the conversion of epichlorohydrin was high up to 98%, which matched well with that obtained in the case of the reported HMOFs (Table S1, ESI†). These results indicate that **3a** and the co-catalyst have a synergistic effect, which can significantly improve the catalytic activity. In order to study the catalytic properties of **3a**, epoxy substrates of different sizes were selected. The results indicated that small butane epoxy leads to a higher yield in the reaction (98%), and the yield of butyl glycidyl ether is ordinary (56%); however, when styrene oxide was used as a substrate, the catalytic conversion was lower (26%), indicating that a smaller epoxy substrate can easily diffuse and interact with the open metal sites in the framework.

Based on the reported cycloaddition mechanism of MOFs as catalysts, it is proposed that there may be two types of reaction mechanisms in this study.[17,18] In the first mechanism, the oxygen atom of the epoxy substrate interacts with the bimetallic Lewis acids (Scheme S2a, ESI†). Simultaneously, Br^- of TBAB attacks the less hindered carbon atoms in the epoxy substrate; this leads to the ring opening of the epoxy substrate and the formation of an active oxygen anion. Finally, the reaction of the active oxygen anion with CO_2 forms alkyl carbonate anions, and the ring-closing reaction produces the corresponding cyclic carbonate and the next reaction catalyst. The second possible mechanism is as follows (Scheme S2b, ESI†). The oxygen atom

of the substrate interacts with the center of the bimetallic ions, and simultaneously, the carbon dioxide molecule is polarized by the base in the HMOF **3** to transform the oxygen atom of CO_2 into an oxygen anion. Then, the oxygen anion attacks the less sterically hindered carbon atoms in the epoxide to form an alkyl carbonate anion, and finally, the ring is closed to form a product and a catalyst for the reaction.[19–21]

Due to the stereochemical activity and strong charge transfer properties of Pb(II) ions, Pb-based MOFs often show novel photochemical performances in the solid state, especially for fine-tuning different color regulations.[22,23] The central metal ions can play a particularly important role as a multiple emission source of photoluminescence. In this study, the three kinds of solid MOFs showed different colors under a UV light of 365 nm at room temperature (Fig. S7a, ESI†). The free ligand has a weak luminescence at 365 nm excitation, and its emission wavelength is 405 nm, resulting from the $\pi^* \rightarrow \pi$ or $\pi^* \rightarrow n$ transition in the ligand. The monometallic Zn-based MOF **1** shows a strong blue emission, and the Pb-based MOF **2** shows a weak yellow emission; the excitation wavelengths of **1** and **2** are 340 nm and 365 nm, respectively, and the corresponding maximum emission peaks are 445 nm and 525 nm. Interestingly, the HMOF **3** shows a near white fluorescence, which can be observed with the naked eyes, due to the combination of Pb(II) and Zn(II) ions, and the HMOF **3** shows two continuous emission peaks at 427 nm and 494 nm (λ_{ex} = 365 nm). The strong fluorescence intensity of **3** should be attributed to the increased rigidity of the ligands after coordination between the bimetallic nodes and H_2L. Compared with the case of the H_2L ligand, the maximum emissions of **1–3** are significantly red shifted; this may be ascribed to metal–ligand charge transfer (MLCT).[18] It can be concluded that the introduction of a second luminescence center into the MOFs can modulate the single-phase photoluminescence to provide a pathway for the fine-tuned light source.

In addition, the emission intensity, spectral shape, and maximum peak position of **3** were further investigated at different excitation wavelengths. In the wide excitation range of 320–450 nm, the fluorescence of **3** confirmed its large Stokes-shifted broadband emission covering the big range of the visible spectrum (from 380 to 700 nm) (Fig. S7b, ESI†). The emission intensity increased by about 6 times at 450 nm excitation as compared to that at 320 nm excitation. It should be noted that under the excitation of 370 nm, the emission spectra of **3** had a large full-width-at-half-maximum (FWHM), which was up to 171 nm (Fig. S8, ESI†). It is found that an In-based SMOF-1 exhibited an intrinsic broadband white emission; however, its FWHM was relatively narrow (150 nm).[24] The fact that this broadband white emission was rare in fluorescent MOFs implies that **3** may be a promising photoemitter for industrial applications.

In summary, herein, three new MOFs were systematically synthesized, in which the MOFs **1** and **2** are monometallic 3D packed frameworks, whereas HMOF **3** is a porous 3D framework with high-density LBSs and LASs. As a result, the highly stable HMOF **3** shows an enhanced catalysis for CO_2, and the fine color regulations of MOFs were also successfully realized by doping different ions. This work will provide an effective mean for building different functional HMOFs *via* a facile one-step synthesis strategy. Subsequently, these emerging HMOF materials will be promising candidates for wide applications in the field of industrially important CO_2 conversion and photoemitters in the near future.

This work was supported by the NSFC (21531007, 21971207 and 21801111), the Project of Central Plains Science and Technology Innovation Leading Talents of Henan Province (204200510001), the Key Science and Technology Innovation Team of Shaanxi Province (2019TD-007), and the NSF of Shaanxi Province (2019JM-013).

Conflicts of interest

There are no conflicts to declare.

Notes and references

1 S. Abednatanzi, P. G. Derakhshandeh, H. Depauw, F.-X. Coudert, H. Vrielinck, P. V. D. Voort and K. Leus, *Chem. Soc. Rev.*, 2019, **48**, 2535–2565.
2 Y.-X. Tan, F. Wang and J. Zhang, *Chem. Soc. Rev.*, 2018, **47**, 2130–2144.
3 L. Liang, C. Liu, F. Jiang, Q. Chen, L. Zhang, H. Xue, H.-L. Jiang, J. Qian, D. Yuan and M. Hong, *Nat. Commun.*, 2017, **8**, 1233–1243.
4 Q.-G. Zhai, X. Bu, C. Mao, X. Zhao and P. Feng, *J. Am. Chem. Soc.*, 2016, **138**, 2524–2527.
5 H. Xu, C.-S. Cao, H.-S. Hu, S.-B. Wang, J.-C. Liu, P. Cheng, N. Kaltsoyannis, J. Li and B. Zhao, *Angew. Chem., Int. Ed.*, 2019, **58**, 6022–6027.
6 J. F. Kurisingal, R. Babu, S.-H. Kim, Y. X. Li, J.-S. Chang, S. J. Cho and D.-W. Park, *Catal. Sci. Technol.*, 2018, **8**, 591–600.
7 L. Wang, C. Xu, Q. Han, X. Tang, P. Zhou, R. Zhang, G. Gao, B. Xu, W. Qin and W. Liu, *Chem. Commun.*, 2018, **54**, 2212–2215.
8 E.-C. Yang, J. Li, B. Ding, Q.-Q. Liang, X.-G. Wang and X.-J. Zhao, *CrystEngComm*, 2008, **10**, 158–161.
9 J. He, M. Zeller, A. D. Hunter and Z. Xu, *J. Am. Chem. Soc.*, 2012, **134**, 1553–1559.
10 M. Fang and B. Zhao, *Rev. Inorg. Chem.*, 2015, **35**, 81–113.
11 V. A. Blatov, http://www.topos.ssu.samara.ru, 2007.
12 J. Lan, Y. Qu, X. Zhang, H. Ma, P. Xu and J. Sun, *J. CO2 Util.*, 2020, **35**, 216–224.
13 P.-Z. Li, X.-J. Wang, J. Liu, J. S. Lim, R. Zou and Y. Zhao, *J. Am. Chem. Soc.*, 2016, **138**, 2142–2145.
14 Y.-Z. Chen, R. Zhang, L. Jiao and H.-L. Jiang, *Coord. Chem. Rev.*, 2018, **362**, 1–23.
15 L. Wang, C. Xu, Q. Han, X. Tang, P. Zhou, R. Zhang, G. Gao, B. Xu, W. Qin and W. Liu, *Chem. Commun.*, 2018, **54**, 2212–2215.
16 R. Zou, P.-Z. Li, Y.-F. Zeng, J. Liu, R. Zhao, H. Duan, Z. Luo, J.-G. Wang, R. Zou and Y. Zhao, *Small*, 2016, **12**, 2334–2343.
17 K. Xu, A. M. P. Moeljadi, B. K. Mai and H. Hirao, *J. Phys. Chem. C*, 2017, **122**, 503–514.
18 J. Kim, S.-N. Kim, H.-G. Jang, G. Seo and W.-S. Ahn, *Appl. Catal., A*, 2013, **453**, 175–180.
19 T. Ema, Y. Miyazaki, S. Koyama, Y. Yano and T. Sakai, *Chem. Commun.*, 2012, **48**, 4489–4491.
20 J. Lan, M. Liu, X. Lu, X. Zhang and J. Sun, *ACS Sustainable Chem. Eng.*, 2018, **6**, 8727–8735.
21 Y. Li, X. Zhang, P. Xu, Z. Jiang and J. Sun, *Inorg. Chem. Front.*, 2019, **6**, 317–325.
22 Z. Yin, W.-M. Ma, C. Wang, X.-P. Luo, X.-T. Hu, L.-H. Cao, X.-Y. Li, X.-Y. Yu, Y.-M. Ma and M.-H. Zeng, *Inorg. Chem.*, 2019, **58**, 16171–16179.
23 R.-W. Huang, X.-Y. Dong, B.-J. Yan, X.-S. Du, D.-H. Wei, S.-Q. Zang and T. C. W. Mak, *Angew. Chem., Int. Ed.*, 2018, **57**, 8560–8566.
24 C. Wang, Z. Yin, W.-M. Ma, X.-Y. Li, L.-H. Cao, Y. Cheng, X.-Y. Yu and Y.-M. Ma, *Dalton Trans.*, 2019, **48**, 14966–14970.